Photoinduced Dynamics of Formic Acid Monomers and Dimers: The Role of the Double Hydrogen Bond

ARTICLE *in* THE JOURNAL OF PHYSICAL CHEMISTRY A · SEPTEMBER 2012

Impact Factor: 2.69 · DOI: 10.1021/jp3074865 · Source: PubMed

THE JOURNAL OF PHYSICAL CHEMISTRY A

Article

pubs.acs.org/JPCA

Photoinduced Dynamics of Formic Acid Monomers and Dimers: The Role of the Double Hydrogen Bond

Jurica Novak,[†] Momir Mališ,[†] Antonio Prlj,[‡] Ivan Ljubić,[†] Oliver Kühn,[§] and Nađa Došlić*,[†]

[†]Rudjer Bošković Institute, 10000 Zagreb, Croatia

[‡]Faculty of Science, University of Zagreb, 10000 Zagreb, Croatia

[§]Institut für Physik, Universität Rostock, D-18051 Rostock, Germany

ABSTRACT: Nonadiabatic dynamics in the framework of time-dependent density functional theory was used to simulate gas-phase relaxation dynamics of pairs of conformations of formic acid monomers (cis and trans FAM) and dimers (acyclic aFAD and cyclic cFAD). In the early phase of the excited state dynamics, elongation of the C═O bond and pyramidalization of the carbon atom is observed in both FAM and FAD. Subsequently, the photodynamics of FAM is shown to be dominated by fragmentation processes occurring mostly in the excited state and resulting in HCO and OH radicals. In only a few cases does the dissociation take place from the vibrationally excited ground electronic state, whereby CO and H_2O are the major reaction products. In the dimers, single proton transfer triggers ultrafast relaxation to the ground electronic state. In the single hydrogen bonded dimer about half of the trajectories dissociate into electronically excited monomers, whereas this potentially destructive dissociation is effectively suppressed in the double hydrogen bonded dimer. Upon relaxation to the ground electronic state, separation of FAD into monomers takes place, but without their further fragmentation on the time scale of the simulation. We conclude that the crucial difference between the FAM and FAD photodynamics is that the latter is dominated by nondestructive radiationless deactivation pathways during which a key protective role is assumed by the single (aFAD) or double (cFAD) intermonomer hydrogen bonds.

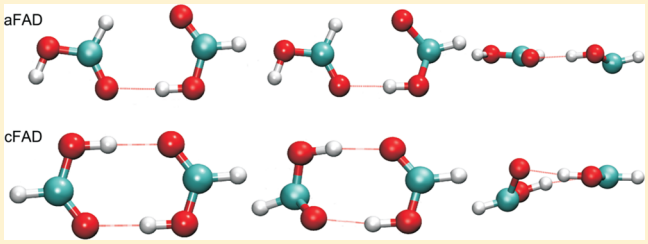

1. INTRODUCTION

Hydrogen bonds (HBs) play a key role in the structure and dynamics of chemical and biological systems.[1−3] A binding motif of particular importance is the double HB, with DNA base pairing being the most prominent example. Due to their simplicity cyclic carboxylic acid dimers are often taken as prototype systems for studying double HB dynamics. Here, the cyclic formic acid dimer (cFAD), as the smallest example, has been a subject of extensive experimental[4−7] and theoretical investigations.[8−13] However, all of these studies have focused solely on the ground electronic state. Of particular interest were the anharmonic couplings and Fermi resonances, giving rise to the broadening and red shift of the infrared active OH stretching vibration[5,14−16] on the one hand, and the proton transfer tunneling splittings in the ground and vibrationally excited states on the other hand.[13,17−23]

Despite the prototype character of cFAD, there are only a few reports on the excited state properties of this system. The absorption spectrum of cFAD has been measured in the wavelength region of 210−125 nm.[24,25] The weak absorption at 210 nm was assigned to a $n_{2O} \rightarrow \pi^*_{CO}$ transition, whereas a broad and intense absorption originating at around 160 nm was assigned to a $\pi_{CO} \rightarrow \pi^*_{CO}$ transition. Apart from an early work of Morokuma et al.,[26] we are aware of only two computational studies of the FAD absorption spectrum.[27,28] Lourderaj et al.[27] carried out a comparative study of vertical excitation energies. Focusing on the three lowest-lying states they have shown that time-dependent density functional theory (TDDFT) with the B3LYP functional provides good estimates for the experimental excitation energies. Very recently a set of benchmark multistate complete active space second-order perturbation theory (MS-CASPT2) excitation energies has been reported.[28] By covering the entire region between 125 and 200 nm, Cimas et al. confirmed the experimental assignments.[28] However, apart from the work of Singleton et al.,[29] there are neither experimental nor theoretical data available on the photoinduced dynamics of cFAD. This is surprising, given the fact that there has been substantial work devoted to larger base pair mimicking systems like 2-aminopyridine clusters[30] or the 7-azaindole dimer.[31−33]

In contrast to the dimer, the photoinduced dynamics of the formic acid monomer (FAM) has been intensively studied.[24,29,34−37] Upon excitation in the wavelength region between 240 and 190 nm FAM undergoes photodecomposition via three major channels:

$$HCOOH \rightarrow HCO + OH \quad (1)$$

$$HCOOH \rightarrow CO + H_2O \quad (2)$$

Special Issue: Jörn Manz Festschrift

Received: July 28, 2012
Revised: September 25, 2012
Published: September 25, 2012

$$HCOOH \rightarrow CO_2 + H_2 \quad (3)$$

Jolly et al.[34] used laser induced fluorescence (LIF) to show that upon excitation at 222 nm the photodissociation of FAM occurs primarily through the radical channel (1), giving OH with a quantum yield of $\Phi = 0.7$. On the other hand, after photodissociation at 193 and 248 nm vibrationally excited CO, CO_2, and H_2O were detected by time-resolved Fourier transform infrared spectroscopy.[36] This suggests that FAM dissociation takes place either in the excited state via channel (1) and subsequent radical recombination on the ground state surface or by internal conversion to the ground state and subsequent molecular decomposition via channels 2 and 3. A detailed theoretical analysis revealed that upon excitation at 248 nm FAM decays mainly via S_1-S_0 internal conversion and subsequent molecular elimination reactions 2 and 3, whereas the direct dissociation channel (1) dominates at higher excitation energies.[38] This picture was confirmed by direct dynamics calculations.[39] A hint on the photodissociation of FAD was obtained from pressure dependent measurements in which the monomer/dimer ratio was modified. Singleton et al.[29] concluded that (1) is not the major dissociation channel of FAD as a quantum yield of only $\Phi = 0.15$ was found for OH. The question of what is the main photodissociation channel of FAD is thus still unanswered.

The present investigation aims at answering this question. In more general terms, we wish to distill the contribution of the two HBs to the photoinduced dynamics of cFAD. To this end, we compare the photoinduced dynamics of four model systems: the cis and trans formic acid monomers, the cyclic dimer, cFAD, as well as the acyclic formic acid dimer (aFAD), exhibiting a single O−H···O HB only. These systems have been studied by using nonadiabatic dynamics simulations in the framework of TDDFT.[40−47] The nonadiabatic transitions between electronic states were treated by surface hopping. The full-dimensionality of "on-the-fly" nonadiabatic dynamics and the low-dimensionality of the systems together permit a detailed analysis of the atomic motion as well as of the associated molecular orbital changes that are taking place after photoexcitation.

In the next section we summarize the methodology used in this work, the selected electronic structure methods, and the nonadiabatic dynamics approach. Section 3.1 presents the study of the photoinduced dynamics of the formic acid monomers, and the influence of the hydrogen bond formation on the photodynamics of the two formic acid dimers is given in section 3.2. Finally, we summarize the paper and give an outlook in section 4.

2. COMPUTATIONAL METHODS

2.1. Electronic Structure Methods. The singlet vertical valence excitation energies of the cis and trans conformers of FAM were obtained using the multireference CASSCF/CASPT2 approach[48,49] on the MP2/6-311++G(3df,2p) optimized geometries. The relatively small size and the C_s symmetry of FAM allows for the nearly definite CASSCF/CASPT2 results; i.e., it enables the use of an extensive (full-valence) CASSCF active space and a large basis set. The active space consists of 18 active electrons in 14 active orbitals, 10 of them belonging to the A′ and 4 to the A″ irreducible representation. The occupied portion comprises all the p and s bonding interactions as well as the in-plane and out-of-plane lone pairs on the two O atoms. The A′ virtual space includes the σ^*(O−H), σ^*(C−H), and σ^*(C−OH) antibonding orbitals, and the A″ virtual space the antibonding π^*(C−O) plus an additional orbital to correlate the out-of-plane oxygen lone pairs. State-averaged CASSCF (SA-CASSCF) calculations were performed over the six lowest equally weighted CASSCF roots per symmetry species and the Dunning's standard cc-pVTZ basis set[50] was used. The dynamic electron correlation was included via the multistate multireference perturbation treatment to the second-order (MS-CASPT2)[51] taking the 6 SA-CASSCF roots as the zero-order references. The 1s core orbitals on the C and the O atoms were kept frozen; i.e., they were not correlated. We used the IPEA zero-order Hamiltonian with the recommended value of the IPEA shift of 0.25 au.[52] An additional imaginary level shift (ILS)[53] of 0.1 au in the energy denominators proved necessary to eliminate the intruders emerging in the higher-lying states (>9 eV) and to boost the reference weights in all the excited states close to the ground state value.

The vertical excitation energies in FAM and FAD were also calculated via the coupled cluster method to the second order[54] with the resolution of identity approximation (RI-CC2)[55,56] and the TZVP basis set as well as via the TDDFT approach based on the Perdew−Burke−Ernzerhof (the PBE0 variant)[57−60] hybrid functional and the aug-cc-pVDZ basis set. MOLCAS, version 6.4, was used for the CASSCF/CASPT2, and TURBOMOLE, version 6.4, was used for the RI-CC2 and TDPBE0 calculations.[61,62]

2.2. Nonadiabatic Dynamics with Surface Hopping. The nonadiabatic (NA) simulations were performed within the framework of TDDFT[42−44] using Tully's fewest switching surface hopping procedure.[63] We make use of a homemade code coupled to Turbomole 6.4 based on the localized Gaussian basis sets approach proposed by Mitrić et al.[45,46,64] In the following, a brief overview of the method is given with emphasis on some aspects of the numerical implementation.

In NA dynamics the electrons are treated quantum mechanically and the nuclei classically. The electronic wave function, $|\Psi(\mathbf{r};\mathbf{R}(t))\rangle$, which depends on the electronic coordinates, $\mathbf{r}$, and parametrically on the nuclear coordinates, $\mathbf{R}$, is expanded in a set of N adiabatic electronic states $|\Psi(\mathbf{r};\mathbf{R}(t))\rangle$ ($j = 1, ..., N$) with time-varying coefficients $C_j(t)$

$$|\Psi(\mathbf{r};\mathbf{R}(t))\rangle = \sum_j C_j(t)|\psi_j(\mathbf{r};\mathbf{R}(t))\rangle \quad (4)$$

The time evolution of the coefficients is given by the time dependent Schrödinger equation:

$$i\hbar\frac{dC_i(t)}{dt} = \sum_j^N C_j(t)(\langle\psi_i(\mathbf{r};\mathbf{R}(t))|\hat{H}_{el}|\psi_j(\mathbf{r};\mathbf{R}(t))\rangle - i\hbar D_{ij})$$
$$= C_i(t)V_{el}^i - i\hbar\sum_j^N C_j(t)D_{ij} \quad (5)$$

where V_{el}^i is the adiabatic energy of the electronic state i and D_{ij} is the element of the nonadiabatic coupling matrix defined as

$$D_{ij} = \left\langle \psi_i(\mathbf{r};\mathbf{R}(t)) \middle| \frac{\partial\psi_j(\mathbf{r};\mathbf{R}(t))}{\partial t} \right\rangle \quad (6)$$

The energies and the gradients, needed for the propagation of the classical trajectories

Table 1. Comparison between the MS-CASPT2(18,14)/cc-pVTZ, RI-CC2/TZVP, and TDPBE0/aug-cc-pVDZ Singlet Valence Spectra for the Trans Isomer of Formic Acid at the MP2/6-311++G(3df,2p) Optimized Geometries[a]

state	dominant coefficients	approx MO interpretation	MS-CASPT2	RI-CC2	TDPBE0
1A′	−0.93971				
2A′	0.78767	$n(2O) \rightarrow \sigma^*(OH)$	8.22	8.16	7.38
	0.47013	$\pi(CO)(-n_z(O)) \rightarrow \pi^*$ (CO)			
3A′	−0.60604	$n(2O) \rightarrow \sigma^*(CH)$	8.97	8.99	7.89
	−0.54493	$\pi(CO)(-n_z(O)) \rightarrow \pi^*(CO)$			
	0.40811	$n(2O) \rightarrow \sigma^*(OH)$			
4A′	0.70696	$n(2O) \rightarrow \sigma^*(CH)$	9.69	9.42	8.56
	−0.49914	$\pi(CO)(-n_z(O)) \rightarrow \pi^*(CO)$			
1A″	−0.84630	$n(2O) \rightarrow \sigma^*(CO)$	6.02	6.07	5.78
	−0.41027	$\sigma(CO,COH) \rightarrow \pi^*(CO)$			
2A″	0.91328	$\pi(CO)(-n_z(O)) \rightarrow \sigma^*(OH)$	9.28	9.13	8.31
3A″	0.83915	$\sigma(CO,COH) \rightarrow \pi^*(CO)$	9.77	9.84	9.29
	−0.35451	$n(2O) \rightarrow \pi^*(CO)$			
4A″	0.93029	$\pi(CO)(-n_z(O)) \rightarrow \sigma^*(OH)$	11.00	11.01	

[a]The excitation energies are given in electronvolts.

$$\mathbf{m}\frac{\mathrm{d}^2\mathbf{R}(t)}{\mathrm{d}t^2} = -\nabla V_{\mathrm{el}}^{j}(\mathbf{R}(t)) \tag{7}$$

are provided by the TDDFT method.

The choice of TDDFT makes the computation of the energy levels and gradients numerically feasible for large molecular systems but complicates the evaluation of (6) as the nonadiabatic couplings, D_{ij}, are defined in terms of electronic wave functions. To compute the nonadiabatic couplings in the framework of TDDFT, we use the method developed by Tavernelli et al.[42−44] and construct a set of "auxiliary" multideterminantal electronic wave functions based on Kohn−Sham (KS) orbitals

$$|\psi_j(\mathbf{r};\mathbf{R}(t))\rangle = \sum_{i,a} c_{\mathrm{i,a}}^{j}\frac{1}{\sqrt{2}}(|\Phi_{\mathrm{i},\alpha}^{a,\beta}(\mathbf{r};\mathbf{R}(t))\rangle + |\Phi_{\mathrm{i},\beta}^{a,\alpha}(\mathbf{r};\mathbf{R}(t))\rangle) \tag{8}$$

where $c_{\mathrm{i,a}}^{j}$ are the expansion coefficients and $|\Phi_{\mathrm{i},\alpha}^{a,\beta}(\mathbf{r};\mathbf{R}(t))\rangle$ and $|\Phi_{\mathrm{i},\beta}^{a,\alpha}(\mathbf{r};\mathbf{R}(t))\rangle$ are singly excited Slater determinants constructed from the occupied (i) and unoccupied (a) set of the KS orbitals. The KS orbitals are in turn given in terms of molecular orbitals (MO) coefficients and Gaussian basis functions.[45,46] Note also that expansion (8) allows the computation of nonadiabatic coupling between pairs of singly excited electronic states with the same multiplicity.[65]

Both $c_{\mathrm{i,a}}^{j}$ and the MO coefficients, are given in the output of Turbomole 6.4, which allows the reconstruction of the "auxiliary" wave function (8) and the evaluation of the nonadiabatic couplings (6). Both sets of coefficients are results of matrix diagonalizations and thus are given up to a sign that needs to be adjusted to construct a smoothly varying $|\Psi_j(\mathbf{r};\mathbf{R}(t))\rangle$.[66]

The NA-TDDFT simulations were performed by using the PBE0 exchange correlation functional and the aug-cc-pVDZ basis set.[60] The velocity Verlet algorithm with the time step of Δt = 0.33 fs was used to integrate the nuclear equations of motion, and the fourth-order Runge−Kutta method was used to obtain the expansion coefficients, $C_j(t)$, required for the computation of the hopping probabilities[42,45,63]

$$P_{j\rightarrow k}(t) = -2\Delta\tau\frac{\mathrm{Re}(C_k^*(t)\, C_j(t)\, D_{kj}(\mathbf{R}(t)))}{C_j^*(t)\, C_j(t)} \tag{9}$$

on the time scale of electronic dynamics $\Delta\tau = \Delta t/(5 \times 10^3)$.

3. RESULTS AND DISCUSSION

3.1. Formic Acid Monomers. To gain a better insight into the performance of the TDPBE0/aug-cc-pVDZ method used later in the nonadiabatic dynamics, we compare CASPT2, RICC2, and TDPBE0 vertical valence spectra of the trans and cis isomers of FAM. At the MP2/6-311++G(3df,2p) and CASPT2(18,14)/cc-pVTZ levels the energy difference between the two conformers is 4.3 and 6.0 kcal mol^{-1}, respectively, in favor of the trans conformer. Tables 1 and 2 compile the MS-CASPT2(18,14)/cc-pVTZ, RI-CC2/TZVP, and TDPBE0/aug-cc-pVDZ singlet valence spectra for the trans and cis conformers, respectively.

It can be concluded that the cis spectrum is systematically red-shifted with respect to the trans, although the transitions in the two conformers are not entirely analogous, being only approximately comparable according to the dominant contributions. A qualitative explanation for the differences in the spectra and dominant contributions can be given on basis of the analysis of the one-electron (SCF) orbitals and energies, which show dissimilarities in the A′ symmetry set, namely overall subtle lowering of the σ skeleton and, most importantly, a pronounced destabilization of the σ^*(OH) LUMO in trans FAM. Conversely, the energies of the matching A″ orbitals differ negligibly between the two conformers.

A satisfactory agreement is found between the CASPT2 and RI-CC2 spectra, especially for trans FAM and "clean", i.e., unmixed, transitions that display a dominant contribution from a single configuration. It shows that both methods, provided adequate basis sets (and the active space in case of CAS) are used, perform similarly and could be deemed accurate enough as to be suitable for assessing other approaches in case of the FAM spectrum. Although the TDPBE0/aug-cc-pVDZ method for the most part keeps the right ordering of the excited states and the agreement with MS-CASPT2 is satisfactory for the lowest states of both conformers, higher-lying states tend to be significantly underestimated by 0.9 eV on average if the comparison is extended to all the calculated roots (6 per A′ and

dx.doi.org/10.1021/jp3074865 | J. Phys. Chem. A 2012, 116, 11467−11475

Table 2. Comparison between the MS-CASPT2(18,14)/cc-pVTZ, RI-CC2/TZVP, and TDPBE0/aug-cc-pVDZ Singlet Valence Spectra for the Cis Isomer of Formic Acid at the MP2/6-311++G(3df,2p) Optimized Geometries[a]

state	dominant coefficients	approx MO interpretation	MS-CASPT2	RI-CC2	TDPBE0
1A′	0.92771				
2A′	−0.88599	$n(2O) \rightarrow \sigma^*(OH)$	7.98	7.68	6.93
3A′	−0.92208	$n(2O) \rightarrow \sigma^*(CH)$	8.34	8.74	7.86
4A′	0.59369	$\pi(CO)(-n_z(O)) \rightarrow \pi^*(CO)$	9.53	9.28	8.54
	−0.53141	$\sigma(CO,COH) \rightarrow \sigma^*(OH)$			
5A′	0.61707	$\sigma(CO,COH) \rightarrow \sigma^*(OH)$	10.76	10.62	
	0.51724	$\pi(CO)(-n_z(O)) \rightarrow \pi^*(CO)$			
1A″	−0.85977	$n(2O) \rightarrow \pi^*(CO)$	5.85	5.96	5.68
2A″	−0.92264	$\pi(CO)(-n_z(O)) \rightarrow \sigma^*(OH)$	8.65	8.55	7.93
3A″	0.90371	$\sigma(CO,COH) \rightarrow \pi^*(CO)$	9.64	9.80	8.63
4A″	0.88822	$\pi(CO)(-n_z(O)) \rightarrow \sigma^*(CH)$	10.52	10.54	

[a]The excitation energies are given in electronvolts.

A″ symmetries). However, as the TDPBE0/aug-cc-pVDZ based NA dynamics is presently aimed at providing insights into FAM photodynamics upon excitation to the lowest excited state ($n_{2O} \rightarrow \pi^*_{CO}$), we expect it not to be seriously affected by these discrepancies.

The adiabatic excitation energies of the cis and trans forms computed at the RI-CC2/TZVP (TDPBE0/aug-cc-pVDZ) level are at 4.53 (4.99) eV and 4.59 (5.08) eV, respectively, i.e., more than 1.3 eV below the vertical excitation. At the S_1 minimum geometry both isomers become nonplanar, characterized by OOCH dihedral angle of 137.0 and 132.7° in the cis and trans forms, respectively.

To simulate the FAM photodecomposition at 222 nm (5.59 eV),[34] we launched an ensemble of 150 initially cis and 150 initially trans FAM trajectories from the S_1 state (1 A″). The initial conditions have been sampled from 15 ps long, room temperature ground state trajectories for the two isomers computed at the RI-PBE/SVP level. The trajectories have been propagated in a subspace spanned by the ground and six lowest excited electronic states. The NA dynamics has been followed for 3 ps.

Figure 1 displays the time variation of the average population of the involved electronic states, i.e., the portion of trajectories residing in each electronic state during the propagation. It is apparent that both conformers exhibit a slow relaxation to the ground state, as after 3 ps only 69 out of 300 trajectories have returned to the ground state. The population decay can be fitted to exponential time constants of 8.5 and 10.8 ps for the cis and trans isomers, respectively. In agreement with the experimental results of Jolly et al.[34] and the direct dynamics study of Martinez-Nunez et al.,[39] we found that channel 1 is the main deactivation mechanism of the S_1 state. A scrutiny of the "reactive" trajectories reveals that C−O bond dissociation accounts for 76% (75%) of the deactivation pathways in the cis (trans) isomers. The remaining "reactive" trajectories return to the ground state without dissociation on S_1, but due to the strong vibrational excitation, the dissociation occurs on S_0. Once on S_0, both sets of trajectories yield predominantly CO + H_2O, whereas CO_2 + H_2 formation was observed in only few cases.

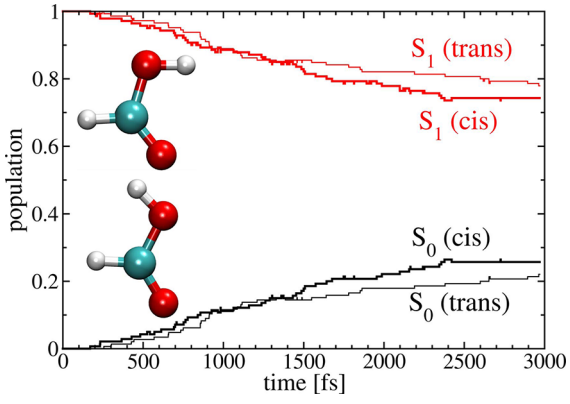

Figure 1. Time dependent populations of the ground and first excited state for the initially cis (thick line) and initially trans (thin line) isomers of FAM. The insets show the ground state structures of trans and cis formic acid.

Figure 2 displays a characteristic nondissociative trajectory on S_1. The first 20 fs of the dynamics are characterized by the out-of-plane motion of the C-bonded hydrogen and elongation of the C═O bond. This leads to the deplanarization of the OOCH moiety and simultaneous destabilization of the ground

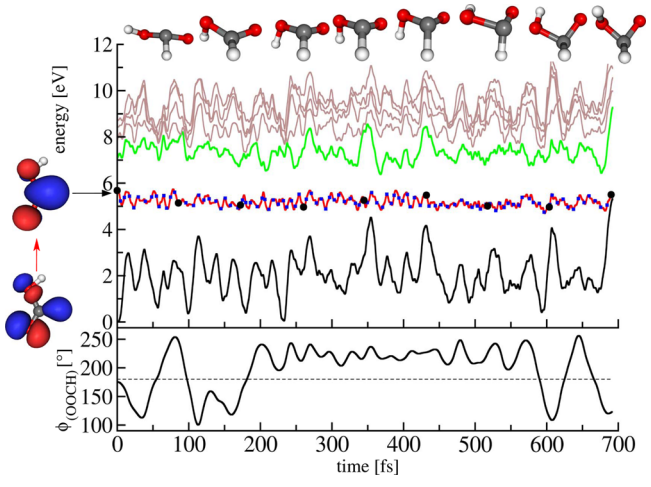

Figure 2. Upper panel: energies of the electronic states along a selected nonadiabatic trajectory of FAM deactivating to S_0 without dissociation on S_1. S_0 is shown in black, S_1 in red, and S_2 in green. Higher excited states are shown in brown. The electronic state in which the trajectory resides is marked with blue dots. The insets show a set of characteristic geometries emphasizing the OH rotation around the C−O bond. Lower panel: time variation of the dihedral angle $\phi_{(OOCH)}$ accounting for the deviation from planarity. The computations have been performed at the TDPBE0/aug-cc-pVDZ level.

dx.doi.org/10.1021/jp3074865 | J. Phys. Chem. A 2012, 116, 11467−11475

state by more than 2.5 eV. The relaxation from the geometry of vertical excitation to a pyramidal structure close to the S_1 minimum supplies to the system ≈1.0 eV of kinetic energy that has to be redistributed between the only 9 vibrational modes. In the present case, apart from the C═O stretch vibration, the umbrella-like motion of the OOCH moiety is excited (Figure 2, lower panel). The deplanarization of the monomer causes strong destabilization of the ground electronic state and the S_1/S_0 conical intersection is reached after 700 fs. The insets along the trajectory show some characteristic geometries. Note the cis/trans isomerization, i.e., the rotation of the OH group around the C—O bond. Our simulations indicate that the lifetime of FAM in the S_1 state is long enough (Figure 1) to ensure a complete randomization of the cis/trans isomerization coordinate. Thus, in contrast to the FAM photodissociation in an Ar matrix, no evidence of conformational memory is expected in the gas phase.[39,67]

The chain of events leading to the C—O bond dissociation is illustrated in Figure 3. The initial dynamics on the S_1 surface

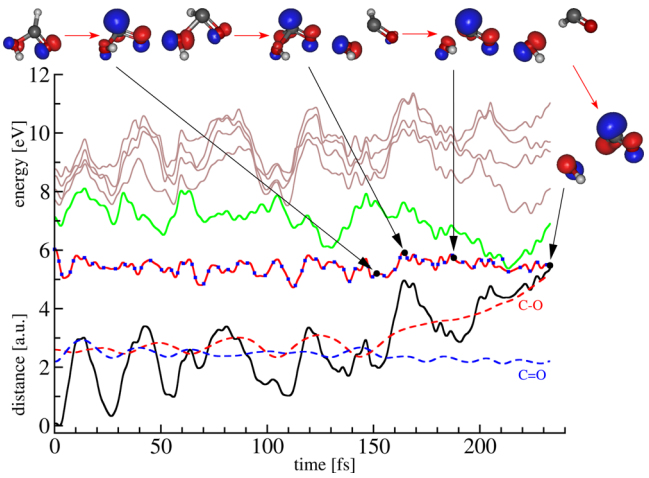

Figure 3. Analysis of a selected nonadiabatic trajectory leading to fragmentation of FAM. Relevant electronic states: S_0 (black), S_1 (red), and S_2 (green). Higher excited states are shown in brown. The electronic state in which the trajectory resides is marked with blue dots. The insets show the leading excitations contributing to S_1. Dashed lines denote the C═O and C—O bond lengths. The computations have been performed at the TDPBE0/aug-cc-pVDZ level.

($n_{2O} \rightarrow \pi^*_{CO}$) is marked by the deplanarization of the OOCH moiety and extension of the C═O bond with simultaneous destabilization of the ground state. The excitation of the C═O and C—O vibrations (scale in au) are shown on top of the variation of the ground state energy. Intramolecular vibrational energy redistribution (IVR) takes place within 80−90 fs as the initial excitation of the C═O oscillator is transferred to the C—O stretching vibration. The amplification of the C—O bond oscillations eventually leads to the dissociation of the C−O bond. The insets along the trajectory show the leading excitation contributing to S_1. Until 160 fs the S_1 state has clear $n_{2O} \rightarrow \pi^*_{CO}$ character. The dissociation of the C—O bond occurs between 170 and 190 fs when the force between the two fragments becomes negligibly small and the fragments separate. Although the reliability of the restricted TDPBE0 description from 190 fs onward could be questionable because of unphysical charge migration, it was shown that the performance of the restricted DFT functionals is satisfactory for bond dissociation curves.[68]

3.2. Formic Acid Dimers. In the following we investigate how the single (aFAD) and double (cFAD) HBs connecting the monomers influence the excited state dynamics. As shown in Figure 4, the ground state minimum energy geometry of aFAD is stabilized by a medium strong O−H···O hydrogen bond (d_{OO} = 2.79 Å) and a weak C−H···O interaction. RI-CC2/TZVP (TDPBE0/aug-cc-pVDZ) yields two close vertical transitions, S_1 at 6.06 (5.78) eV and S_2 at 6.23 (5.99) eV. Both transitions correspond to intramonomer $n_{C=O} \rightarrow \pi^*_{C=O}$ excitations. The absorption spectrum of cFAD is quite similar to that for aFAD. RI-CC2/TZVP (TDPBE0/aug-cc-pVDZ) yielded two almost degenerate transitions S_1 at 6.21 (5.90) eV and S_2 at 6.25 (6.00) eV. Both values compare satisfactory with the reference MS-CASPT2/CASSCF(12,14) excitation energies of 6.13 and 6.21 eV reported by Cimas et al.[28] The rather poor description of charge transfer states by standard DFT functionals shows up in the next state. For S_3 at 6.36 eV TDPBE0/aug-cc-pVDZ gives an intermonomer $n_{2O} \rightarrow \pi^*_{CO}$ transition in aFAD, whereas this transition corresponds to S_5 in the RI-CC2/TZVP spectrum found at 8.66 eV. Due to C_{2h} symmetry in cFAD the distinction between intra- and intermonomer excitations is not possible in the used canonical basis. However, because NA dynamics of both dimers takes place predominantly on S_1 and S_2 (vide infra) the TDPBE0/aug-cc-pVDZ description of the NA dynamics is satisfactory in both cases.

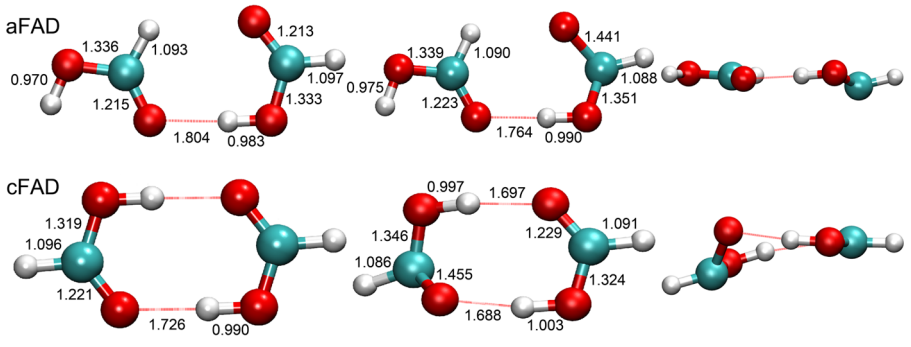

Figure 4. Top: minimum energy geometry of aFAD (right) and two perspectives of the S_1 optimized geometry (center and right). Bottom: minimum energy geometry of cFAD (right) and two perspectives of the S_1 optimized geometry (center and right). Ground state geometries have been computed at the MP2/6-311+G(d,p) level. The S_1 optimized geometries have been computed using the RI-CC2/TZVP method.

dx.doi.org/10.1021/jp3074865 | J. Phys. Chem. A 2012, 116, 11467−11475

At the RI-CC2/TZVP (TDPBE0/aug-cc-pVDZ) level the two lowest triplet states T_1 and T_2 of aFAD are found at 5.69 (5.16) eV and 5.88 (5.37) eV, whereas in cFAD the T_1 state is found at 5.89 (5.34) eV and T_2 at 5.92 (5.40) eV. In the present dynamical approach, switches between PESs of different multiplicity are not allowed. However, in the absence of heavy atoms, it is safe to assume that intersystem crossing takes place on time scales that are longer than those considered here (3 ps).[69]

The minimum geometry of the S_1 state of aFAD is shown in Figure 4 (top, center and right). It corresponds to a structure in which one of the monomers is nonplanar and the other is planar. The S_1 minimum geometry is located 4.58 (5.14) eV above the ground state minimum at RI-CC2/TZVP (TDPBE0/aug-cc-pVDZ), i.e., almost 1.5 eV below the Franck−Condon transition energy. As shown in Figure 4 (bottom, center and right), the S_1 minimum energy structure of cFAD features also a nonplanar and a planar monomer. The RI-CC2/TZVP (TDPBE0/aug-cc-pVDZ) adiabatic excitation energy is 4.58 (5.22) eV. On this basis we can anticipate that the initial dynamics after photoexcitation will be determined by the large difference between the geometry of the vertical excitation and the S_1 optimized geometry.

Let us focus first on the photoinduced dynamics of aFAD. We propagated an ensemble of 100 trajectories in the subspace of the ground and six excited electronic states for a total of 3.0 ps starting from the S_1 state. Figure 5 shows that rather efficient

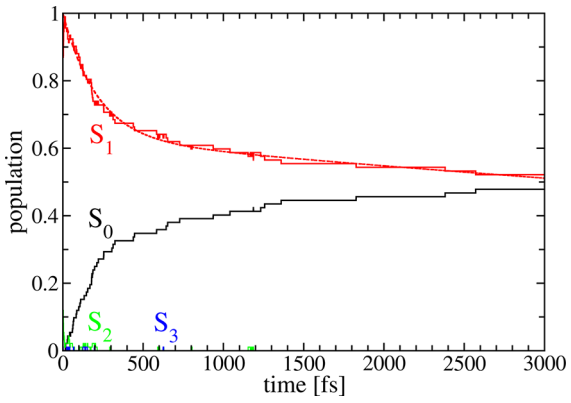

Figure 5. Time dependent population of the ground and excited electronic states of aFAD. S_0 is shown in black, S_1 in red, S_2 in green, and S_3 in blue. The dashed line is the biexponential fit for the decay of S_1 with time constants of 228 fs and 15.1 ps.

relaxation takes place in aFAD because at the end of simulation 48% of the trajectories have returned to the ground state. The difference with respect to FAM photodynamics ought to be connected to the formation of the O−H···O HB. The decay of S_1 includes a dissociative and a nondissociative component. These dissociative trajectories correspond to the dissociation of aFAD on the S_1 surface. The subsequent relaxation of the monomers to the ground state may lead to their fragmentation, but on a much longer time scale than in FAM, as part of the excess vibrational energy is transferred to translation. The decay of the nondissociative trajectories is, in turn, biexponential, with time constants of 228 fs and 15.1 ps. A closer analysis shows that the fast relaxation channel corresponds to proton transfer from the donor monomer (HD) to the electronically excited acceptor monomer (HA), whereas the slow channel encompasses the reorientation of aFAD to form a double hydrogen bonded dimer (cFAD) that then decays to the ground state by proton transfer.

Figure 6 illustrates the fast relaxation mechanism. At the initial geometry, the electronic excitation is localized predom-

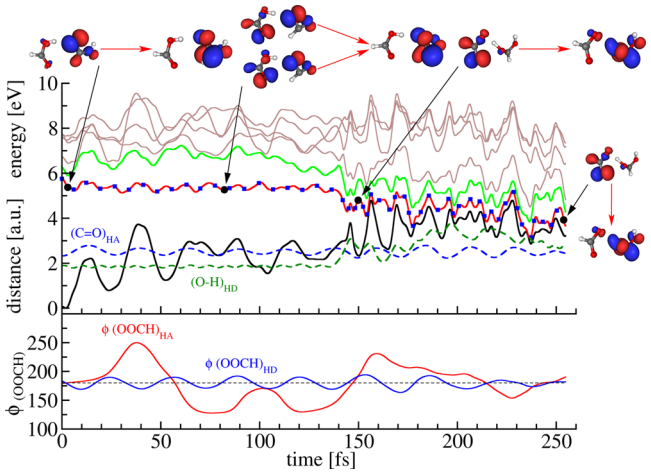

Figure 6. Upper panel: energies of the electronic states along a selected NA trajectory of aFAD. Deactivation to S_0 occurs by single H-transfer. The S_0 state is shown in black, S_1 in red, and S_2 in green. Higher excited states are shown in brown. Blue dots denote the electronic state in which the trajectory resides. The insets show the leading excitations contributing to S_1. The C═O and O—H bond lengths are shown with dashed lines. Lower panel: time variation of the dihedral angle ϕ_{OOCH} of the donor and acceptor monomers.

inantly on the H-accepting monomer. The initial dynamics on the S_1 surface encompasses the extension of the C═O bond and pyramidalization of the C atom of the proton acceptor monomer. The redistribution of the excess kinetic energy into atomic motion yields a vibrationally "hot" monomer within aFAD. The early dynamics of aFAD, hence, closely resembles the monomer dynamics. The difference emerges at 140−150 fs when, instead of energy transfer from C═O stretching to C—O stretching on the same monomer leading to the fragmentation, the vibrational excitation is transferred to the O—H stretching vibration of the other monomer via the HB. The proton transfer, occurring at ≈140 fs, is very unfavorable for the ground state, whose energy strongly rises and the two surfaces cross. Once on the S_0 surface, the backward proton transfer reaction takes place and the two monomers separate.

It has long been proposed that photoinduced proton transfer can play an important role in the efficient excited state deactivation of proteins and DNA.[70−73] Our simulations confirmed the key role of proton transfer in the radiationless deactivation of aFAD. Although aFAD is a small model system, its photodynamics is governed by processes that are analogous to the ones relevant to the excited state deactivation of HB biomolecules. Note also that the photoinduced dynamics of aFAD reveals that single HBs are not sufficient to prevent potentially harmful dissociation in the excited electronic state.

We finally turn to the NA dynamics of the cyclic dimer, cFAD. An ensemble of 100 trajectories has been propagated starting from the first optically allowed state, S_2, for a total of 3 ps. As shown in Figure 7, an almost complete population transfer to the ground state occurs within the propagation time. Virtually no dissociation of cFAD in the S_1 state has been observed. At first glance, the mechanism underlying such efficient relaxation is, as in the case of aFAD, single proton

dx.doi.org/10.1021/jp3074865 | J. Phys. Chem. A 2012, 116, 11467−11475

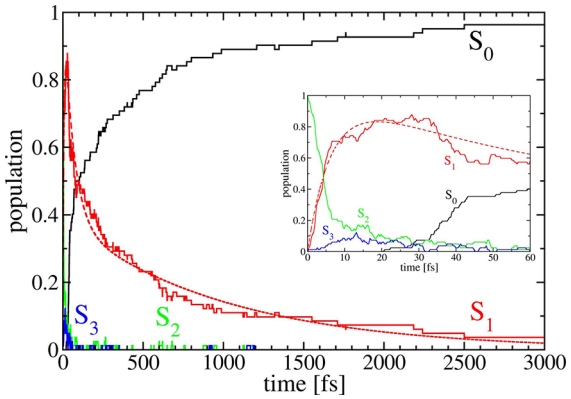

Figure 7. Time dependent population of the ground and excited electronic states of cFAD. S_0 is shown in black, S_1 in red, S_2 in green, and S_3 in blue. The dashed line is the biexponential fit for the population decay of S_1 with time constants of 62 fs and 1.0 ps. The inset shows the initial 60 fs of the nonadiabatic dynamics.

transfer occurring on the S_1 surface. The reaction is, however, more complex as it includes the transfer of the second proton on the S_0 surface. Note also that the initially excited monomer becomes the hydrogen donor (HD) monomer. Figure 8

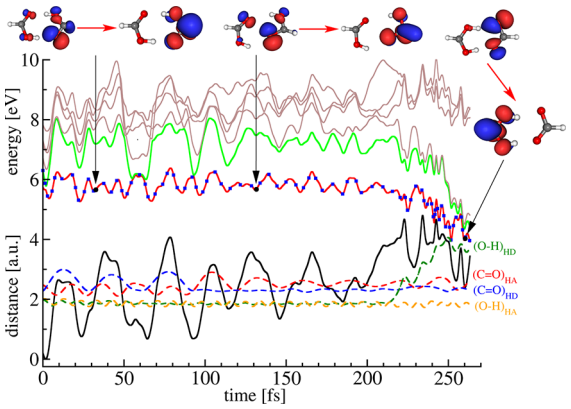

Figure 8. Energies of the electronic states along a selected nonadiabatic trajectory of cFAD. Deactivation to S_0 occurs by excited state proton transfer. The S_0 state is shown in black, S_1 in red, and S_2 in green. Higher excited states are shown in brown. The electronic state in which the trajectory resides is marked with blue dots. The insets show the leading excitations contributing to S_1. Dashed lines denote the two C═O and two O−H bond lengths.

displays the analysis of a representative cFAD trajectory. Up to 80 fs the dynamics closely follow the pattern found for FAM and aFAD: lengthening of the C═O bond and pyramidalization of the HD monomer. A new aspect occurs at ≈90 fs when the excitation is transferred from the C═O stretching vibration of the HD monomer to the C═O stretching vibration of the hydrogen acceptor (HA) monomer. The change of the two C═O bond lengths can be followed in Figure 8 (dashed lines). Finally, the excitation is transferred to the O—H stretching vibration of the HD monomer and the proton transfer takes place, in the present example at 220 fs. This is apparent from the abrupt elongation of the $(O—H)_{HD}$ bond and the change in the energies of the excited electronic states as a zwitterion is formed. A switch to the ground state occurs at 263 fs. By following the dynamics on S_0, within a few femtoseconds, we observed the second proton-transfer reaction, now from $(O—H)_{HA}$. The net result is the re-formation of the initial dimer that subsequently dissociates on the ground state surface.

In general, we found that the initial dimer can be recovered in two ways, either by single or by double proton transfer. In the former case, the same proton is first forward-transferred on S_1 and then back-transferred on S_0, whereas in the latter case one of the protons is forward-transferred on S_1 and the other is back-transferred on S_0. Our study yielded an approximate 2:1 ratio for single vs double proton transfer. In this context it is interesting to note that the concerted double proton transfer, i.e., the mechanism emerging from minimum energy path calculations, has not been observed in the nonadiabatic dynamics simulations. Finally, our study reveals that the resonant energy transfer between two C═O stretching vibrations plays an important step in cFAD deactivation as the vibrational excitation is transferred between the two monomers on the time scale that is faster than IVR. The subsequent proton-transfer reactions complete the deactivation process.

4. SUMMARY AND OUTLOOK

We have carried out a TDPBE0/aug-cc-pVDZ nonadiabatic dynamics simulations of monomeric and dimeric formic acid with the goal of studying the influence of hydrogen bonding on the photodynamics. We have found that in all systems the dynamics right after photoexcitation is characterized by the extension of the C═O bond and pyramidalization of the monomers. In the case of formic acid monomers, the anharmonic coupling between the C═O and C—O stretching vibrations leads predominantly to the fragmentation of the C—O bond on a time scale of ≈10 ps. In contrast, our results show that double, and to a lesser extent single, HB dimers exhibit efficient nonradiative relaxation via photoinduced proton transfer. In both cases virtually no fragmentation of the constituent monomers has been observed. Perhaps, the most important result of our investigation is the mechanism of excited state deactivation in the double hydrogen bonded dimer. As a key step, it encompasses vibrational energy transfer between the two monomers, from the C═O stretching vibration of the electronically excited monomer to the C═O stretching vibration of the other monomer. The relaxation to the electronic ground state occurs by single proton transfer from the electronically excited monomer. To recover the initial dimer, a second proton-transfer reaction takes place in the ground electronic state.

The present investigation can be extended in several ways. In principle, we have treated a quantum system with mixed classical quantum dynamics. The pathways of nonradiative relaxation unravelled by NA-TDDFT simulations need to be reinvestigated using a quantum dynamical method, such as the multiconfiguration time-dependent Hartree approach, for example.[74] Furthermore, it is nowadays accepted that photoinduced proton-transfer reactions provide photostability to hydrogen bonded biomolecules.[75] Even though cFAD is a small model system, the deactivation pathways found in cFAD exhibit close similarity to the mechanisms of excited state deactivation encountered in hydrogen bonded biomolecules. Previous studies have shown that single and double proton transfer are energetically feasible mechanisms of excited state deactivation.[70−73] The present study points to the robustness of these mechanisms. We have shown how the competing mechanism, i.e., dissociation of the dimer on the excited electronic state surface that may eventually lead to fragmentation is effectively

dx.doi.org/10.1021/jp3074865 | J. Phys. Chem. A 2012, 116, 11467−11475

suppressed in the double HB cFAD. In this context it is important to extend the present approach to include the interaction with the environment and open up the way for direct investigation of light induced proton transfer in biological systems.

AUTHOR INFORMATION

Corresponding Author

*E-mail: nadja.doslic@irb.hr.

Notes

The authors declare no competing financial interest.

ACKNOWLEDGMENTS

This work has been financed by the Croatian MZOS projects 098-0352851-2921 and 098-0982915-2944. We gratefully acknowledge financial support by the DAAD and the MZOS within a Croatian-German bilateral project. We also acknowledge the support of the Croatian national grid infrastructure.

REFERENCES

(1) Limbach, H. H.; Manz, J. *Ber. Bunsen-Ges. Phys. Chem.* **1998**, *102*, 289−291.
(2) Hynes, J. T., Klinman, J. P., Limbach, H. H., Schowen, R. L., Eds. *Hydrogen transfer reactions*; Wiley-VCH: Weinheim, 2006.
(3) Giese, K.; Petković, M.; Naundorf, H.; Kühn, O. *Phys. Rep.* **2006**, *430*, 211−276.
(4) Almenningen, A.; Bastiansen, O.; Motzfeld, T. *Acta Chem. Scand.* **1969**, *23*, 2848−2864.
(5) Ito, F.; Nakanaga, T. *Chem. Phys. Lett.* **2002**, *277*, 163−169.
(6) Madeja, F.; Havenith, M. *J. Chem. Phys.* **2002**, *117*, 7162−7168.
(7) Birer, Ö.; Havenith, M. *Annu. Rev. Phys. Chem.* **2009**, *60*, 263−275.
(8) Neuheuser, T.; Hess, B. A.; Reutel, C.; Weber, E. *J. Phys. Chem.* **1994**, *98*, 6459−6467.
(9) Vener, M. V.; Kühn, O.; Bowman, J. M. *Chem. Phys. Lett.* **2001**, *349*, 562−570.
(10) Ushiyama, H.; Takatsuka, K. *J. Chem. Phys.* **2001**, *115*, 5903−5912.
(11) Tautermann, C. S.; Voegele, A. F.; Liedl, K. R. *J. Chem. Phys.* **2004**, *120*, 631−637.
(12) Markwick, P. R. L.; Doltsinis, N. L.; Marx, D. *J. Chem. Phys.* **2005**, *122*, 054112/1−8.
(13) Luckhaus, D. *J. Phys. Chem. A* **2006**, *110*, 3151−3158.
(14) Maréchal, Y. *J. Chem. Phys.* **1987**, *87*, 6344−6353.
(15) Florio, G. M.; Zwier, T. S.; Myshakin, E. M.; Jordan, K. D.; Sibert, E. L., III. *J. Chem. Phys.* **2003**, *118*, 1735−1746.
(16) Matanović, I.; Došlić, N. *Chem. Phys.* **2007**, *338*, 121−126.
(17) Ortlieb, M.; Havenith, M. *J. Phys. Chem. A* **2007**, *111*, 7355−7363.
(18) Mil'nikov, G. V.; Kühn, O.; Nakamura, H. *J. Chem. Phys.* **2005**, *123*, 074308/1−9.
(19) Smedarchina, Z.; Fernandez-Ramos, A.; Siebrand, W. *J. Chem. Phys.* **2005**, *122*, 134309/1−12.
(20) Matanović, I.; Došlić, N.; Kühn, O. *J. Chem. Phys.* **2007**, *127*, 014309/1−7.
(21) Matanović, I.; Došlić, N.; Johnson, B. R. *J. Chem. Phys.* **2008**, *128*, 084103/1−10.
(22) Barnes, G. L.; Sibert, E. L., III. *J. Chem. Phys.* **2008**, *129*, 164317/1−9.
(23) Mališ, M.; Matanović, I.; Došlić, N. *J. Phys. Chem. A* **2009**, *113*, 6034−6040.
(24) Singleton, D. L.; Paraskevopoulos, G.; Irwin, R. S. *J. Phys. Chem.* **1990**, *94*, 695−699.
(25) Mualem, R.; Sominska, E.; Kelner, V.; Gedanken, A. *J. Chem. Phys.* **1992**, *97*, 8813−8814.
(26) Iwata, S.; Morokuma, K. *Theor. Chim. Acta* **1977**, *44*, 323−339.
(27) Lourderaj, U.; Giri, K.; Sathyamurthy, N. *J. Phys. Chem. A* **2006**, *110*, 2709−2717.
(28) Cimas, A.; Mó, O.; Yáñez, M.; Martin, N.; Corral, I. *Phys. Chem. Chem. Phys.* **2010**, *12*, 13037−13046.
(29) Singleton, D. L.; Paraskevopoulos, G.; Irwin, R. S. *Res. Chem. Intermed.* **1989**, *12*, 1−12.
(30) Schultz, T.; Samoylova, E.; Radloff, W.; Hertel, I. V.; Sobolewski, A. L.; Domcke, W. *Science* **2004**, *306*, 1765−1768.
(31) Sekiya, H.; Sakota, K. *Bull. Chem. Soc. Jpn.* **2006**, *79*, 373−385.
(32) Kwon, O.-H.; Zewail, A. H. *Proc. Nat. Acad. Sci. U. S. A.* **2007**, *104*, 8703−8708.
(33) Takeuchi, S.; Tahara, T. *Proc. Nat. Acad. Sci. U. S. A.* **2007**, *104*, 5285−5290.
(34) Jolly, G. S.; Singleton, D. L.; Paraskevopoulos, G. *J. Phys. Chem.* **1987**, *91*, 3463−3465.
(35) Brouard, M.; Wang, J. *J. Chem. Soc., Faraday Trans.* **1992**, *88*, 3511−3516.
(36) Su, H.; He, Y.; Kong, F.; Fang, W.; Liu, R. *J. Chem. Phys.* **2000**, *113*, 1891−1897.
(37) Huang, C.; Zhang, C.; Yang, X. *J. Chem. Phys.* **2010**, *132*, 154306/1−6.
(38) He, H. Y.; Fang, W. H. *J. Am. Chem. Soc.* **2003**, *125*, 16139−16147.
(39) Martinez-Nunez, E.; Vazquez, S. A.; Granucci, G.; Persico, M.; Estevez, C. M. *Chem. Phys. Lett.* **2005**, *412*, 35−40.
(40) Doltsinis, N. L.; Marx, D. *Phys. Rev. Lett.* **2002**, *88*, 166402/1−4.
(41) Craig, C. F.; Duncan, W. R.; Prezhdo, O. *Phys. Rev. Lett.* **2005**, *95*, 163001/1−4.
(42) Tapavicza, E.; Tavernelli, I.; Rothlisberger, U. *Phys. Rev. Lett.* **2007**, *98*, 023001/1−4.
(43) Tavernelli, I.; Tapavicza, E.; Rothlisberger, U. *J. Chem. Phys.* **2009**, *130*, 124107/1−10.
(44) Tavernelli, I.; Curchod, B. F. E.; Rothlisberger, U. *J. Chem. Phys.* **2009**, *131*, 196101/1−2.
(45) Mitrić, R.; Werner, U.; Bonačić-Koutecký, V. *J. Chem. Phys.* **2008**, *129*, 164118/1−9.
(46) Werner, U.; Mitrić, R.; Suzuki, T.; Bonačić-Koutecký, V. *Chem. Phys.* **2008**, *349*, 319−324.
(47) Klaumunzer, B.; Kröner, D.; Lischka, H.; Saalfrank, P. *Phys. Chem. Chem. Phys.* **2012**, *14*, 8693−8702.
(48) Roos, B. O.; Andersson, K.; Fülscher, M. P.; Malmqvist, P.-A.; Serrano-Andrés, L.; Pierloot, K.; Merchán, M. Multiconfigurational perturbation theory: Applications in electronic spectroscopy. In *Advances in Chemical Physics: New Methods in Computational Quantum Mechanics*; Prigogine, I., Rice, S. A., Eds.; John Wiley and Sons: New York, 1996.
(49) Andersson, K.; Malmqvist, P.-A.; Roos, B. O. *J. Chem. Phys.* **1992**, *96*, 1218−1226.
(50) Dunning, T. *J. Chem. Phys.* **1989**, *90*, 1007−1023.
(51) Finley, J.; Malmqvist, P. A.; Roos, B. O.; Serrano-Andrés, L. *Chem. Phys. Lett.* **1998**, *288*, 299−306.
(52) Ghigo, G.; Roos, B. O.; Malmqvist, P. A. *Chem. Phys. Lett.* **2004**, *396*, 142−149.
(53) Forsberg, N.; Malmqvist, P. A. *Chem. Phys. Lett.* **1997**, *274*, 196−204.
(54) Christiansen, O.; Koch, H.; Jorgensen, P. *Chem. Phys. Lett.* **1995**, *243*, 409−418.
(55) Hättig, C.; Weigend, F. J. *J. Chem. Phys.* **2000**, *113*, 5154−5161.
(56) Hättig, C.; Hellweg, A.; Köhn, A. *Phys. Chem. Chem. Phys.* **2006**, *8*, 1159−1169.
(57) Perdew, J. P.; Burke, K; Ernzerhof, M. *Phys. Rev. Lett.* **1996**, *77*, 3865−3868.
(58) Perdew, J. P.; Burke, K; Ernzerhof, M. *Phys. Rev. Lett.* **1997**, *78*, 1396.
(59) Adamo, C.; Barone, V. *J. Chem. Phys.* **1999**, *110*, 6158−6170.
(60) Ciofini, I.; Adamo, C. *J. Phys. Chem. A* **2007**, *111*, 5549−5556.
(61) Karlstrom, G.; Lindh, R.; Malmqvist, P.-A.; Roos, B. O.; Ryde, U.; Veryazov, V.; Widmark, P.-O.; Cossi, M.; Schimmelpfennig, B.; Neogrady, P.; et al. *Comput. Mater. Sci.* **2003**, *28*, 222−239.

(62) Ahlrichs, R.; Bar, M.; Haser, M.; Horn, H.; Kolmel, C. *Chem. Phys. Lett.* **1989**, *162*, 165−169.
(63) Tully, J. *J. Chem. Phys.* **1990**, *93*, 1061−1071.
(64) Mitrić, R.; Petersen, J.; Bonačić-Koutecký, V. Multistate Nonadiabatic Dynamics "on the Fly" in Complex Systems and Its Control by Laser Fieldes. In *Conical Intersections: Theory, Computation and Experiment*; Domcke, W., Yarkony, D., Köppel, H., Eds.; World Scientific: Singapore, 2011.
(65) Tavernelli, I.; Curchod, B. F. E.; Laktionov, A.; Rothlisberger, U. *J. Chem. Phys.* **2010**, *133*, 194104/1−10.
(66) Full, J.; Gonzalez, L.; Manz, J. *Chem. Phys.* **2005**, *314*, 143−158.
(67) Khriachtchev, L.; Macoas, E.; Pettersson, M.; Rasanen, M. *J. Am. Chem. Soc.* **2002**, *124*, 10994−10995.
(68) Menon, A. M.; Wood, G. P. F.; Moran, D.; Radom, L. *J. Phys. Chem. A* **2007**, *111*, 13638−13644.
(69) Cannizzo, A.; van Mourik, F.; Gawelda, W.; Zgrablić, G.; Bressler, C.; Chergui, M. *Angew. Chem., Int. Ed.* **2006**, *45*, 3174−3176.
(70) Sobolewski, A. L.; Domcke, W. *Phys. Chem. Chem. Phys.* **2004**, *6*, 2763−2771.
(71) Lan, Z.; Frutos, L. M.; Domcke, W. *Proc. Natl. Acad. Sci. U. S. A* **2008**, *105*, 12707−12712.
(72) Shemesh, D.; Sobolewski, A. L.; Domcke, W. *J. Am. Chem. Soc.* **2009**, *131*, 1374−1375.
(73) Marazzi, M.; Sancho, U.; Castano, O.; Domcke, W.; Frutos, L. M. *J. Phys. Chem. Lett.* **2010**, *1*, 425−428.
(74) Beck, M. H.; Jäckle, A.; Worth, G. A.; Meyer, H.-D. *Phys. Rep.* **2000**, *324*, 1−105.
(75) Sobolewski, A. L.; Domcke, W. Efficient Excited-State Deactivation in Organic Chromophores and Biologically Relevant Molecules: Role of Electron and Proton Transfer Processes. In *Conical Intersections: Theory, Computation and Experiment*; Domcke, W., Yarkony, D., Köppel, H., Eds.; World Scientific: Singapore, 2011.

■ NOTE ADDED AFTER ASAP PUBLICATION

This paper was published on the Web on October 10, 2012, with an empty reference 1. The empty reference was removed and the citations in the text have adjusted accordingly. The corrected paper was reposted on October 25, 2012.